


# The antiviral potential of the antiandrogen enzalutamide and the viral-androgen signaling interplay in seasonal coronaviruses

Oluwadamilola D. Ogunjinmi<sup>1</sup> | Tukur Abdullahi<sup>1</sup> | Riaz-Ali Somji<sup>1</sup> |  
Charlotte L. Bevan<sup>2</sup> | Wendy S. Barclay<sup>3</sup> | Nigel Temperton<sup>4</sup> | Greg N. Brooke<sup>1</sup> |  
Efstathios S. Giotis<sup>1,3</sup> 

<sup>1</sup>School of Life Sciences, University of Essex, Colchester, UK

<sup>2</sup>Department of Surgery and Cancer, Imperial College London, London, UK

<sup>3</sup>Department of Infectious Diseases, Imperial College London, London, UK

<sup>4</sup>Viral Pseudotype Unit, Medway School of Pharmacy, Universities of Kent and Greenwich, Chatham, UK

## Correspondence

Efstathios S. Giotis, School of Life Sciences, University of Essex, Colchester, UK.  
Email: [e.giotis@essex.ac.uk](mailto:e.giotis@essex.ac.uk)

## Funding information

Nigerian Petroleum Technology Development Fund; University of Essex COVID-19 Rapid and Agile Fund; Faculty of Science and Health Research Innovation and Support Fund; Wellcome Trust, Grant/Award Number: 360G-Wellcome-220981\_Z\_20\_Z

## Abstract

The sex disparity in COVID-19 outcomes with males generally faring worse than females has been associated with the androgen-regulated expression of the protease TMPRSS2 and the cell receptor ACE2 in the lung and fueled interest in antiandrogens as potential antivirals. In this study, we explored enzalutamide, an antiandrogen used commonly to treat prostate cancer, as a potential antiviral against the human coronaviruses which cause seasonal respiratory infections (HCoV-NL63, -229E, and -OC43). Using lentivirus-pseudotyped and authentic HCoV, we report that enzalutamide reduced 229E and NL63 entry and infection in both TMPRSS2- and nonexpressing immortalized cells, suggesting a TMPRSS2-independent mechanism. However, no effect was observed against OC43. To decipher this distinction, we performed RNA-sequencing analysis on 229E- and OC43-infected primary human airway cells. Our results show a significant induction of androgen-responsive genes by 229E compared to OC43 at 24 and 72 h postinfection. The virus-mediated effect on AR-signaling was further confirmed with a consensus androgen response element-driven luciferase assay in androgen-depleted MRC-5 cells. Specifically, 229E induced luciferase-reporter activity in the presence and absence of the synthetic androgen mibolerone, while OC43 inhibited induction. These findings highlight a complex interplay between viral infections and androgen-signaling, offering insights for disparities in viral outcomes and antiviral interventions.

## KEYWORDS

androgen response element, antiandrogens, enzalutamide, SARS-CoV-2, seasonal coronaviruses, TMPRSS2

**Abbreviations:** 229E, human coronavirus 229E; ACE2, angiotensin-converting enzyme 2; ANOVA, analysis of variance; ATCC, American Type Culture Collection; BSL-2, biosafety level 2; CoV, coronavirus; COVID-19, coronavirus disease 2019; GAPDH, glyceraldehyde 3-phosphate dehydrogenase; MOI, multiplicity of infection; NL63, human coronavirus NL63; OC43, human coronavirus OC43; SARS-CoV, severe acute respiratory syndrome coronavirus; TMPRSS2, transmembrane protease serine 2.

This is an open access article under the terms of the [Creative Commons Attribution](https://creativecommons.org/licenses/by/4.0/) License, which permits use, distribution and reproduction in any medium, provided the original work is properly cited.

© 2024 The Authors. *Journal of Medical Virology* published by Wiley Periodicals LLC.

## 1 | INTRODUCTION

Highly pathogenic coronaviruses (CoV), including SARS-CoV, MERS-CoV, and SARS-CoV-2, have caused deadly outbreaks in the 21st century.<sup>1</sup> Four human CoV (HCoV: 229E, NL63, OC43, and HKU1) are endemic globally and cause 10%–20% of seasonal upper respiratory (re-)infections in adults.<sup>2</sup> HCoV-229E and -NL63 are clustered phylogenetically within the genus Alphacoronavirus and emerged in humans from bat populations.<sup>3</sup> Although these viruses are typically associated with the common cold, they can cause severe pneumonia in immunocompromised individuals.<sup>4,5</sup> In addition, NL63 is associated with croup,<sup>6</sup> 229E can cause respiratory distress in healthy adults sporadically,<sup>5</sup> HKU1 typically leads to mild respiratory symptoms, and OC43 is often implicated in severe respiratory infections, especially among vulnerable populations.<sup>4,5</sup> There are currently no prophylactic vaccines or specific antiviral drugs approved for human use against HCoV. Interest in these viruses has been recently renewed as they can be handled in reduced biosafety laboratory containment thus providing an alternative to SARS-CoV-2 for preclinical screening and antiviral design. Furthermore, recent studies reported a possible cross-protective effect of pre-existing HCoV-infection immunity on subsequent SARS-CoV-2 infection and on the severity of COVID-19 outcome.<sup>7</sup>

While there is no explicit report of sexual discordance in HCoV prevalence, it is becoming more evident that males of both younger and older ages are more susceptible to respiratory viruses in general and are also at a higher risk of severe disease outcomes when compared to females.<sup>2</sup> The reasons are not entirely clear, but several explanations have been proposed, including immunological, genetic, hormonal, and socio-behavioral factors.<sup>8</sup> The sex discordance in COVID-19 outcomes, with males generally faring worse than females, has been associated with androgens, the steroid hormones predominant in males, fueling interest in antiandrogens (androgen receptor antagonists) as potential antivirals.<sup>8</sup> We previously demonstrated that enzalutamide, an antiandrogen typically used to prevent the androgen receptor-mediated growth of castrate-resistant prostate cancers, reduces the expression in the lungs and other target cells of the transmembrane serine protease TMPRSS2, a key protease for SARS-CoV-2 cell entry, and thus holds potential as antiviral.<sup>9</sup> TMPRSS2 is part of the type 2 transmembrane serine protease family and has been extensively studied in the context of prostate cancer metastasis.<sup>10</sup> Its expression is upregulated in response to androgens through direct transcriptional regulation by the androgen receptor (AR).<sup>10</sup> Other studies showed that antiandrogens have pleiotropic effects that could also affect viral uptake for example, spironolactone can reduce the expression of the cell surface receptor of SARS-CoV-2 angiotensin-converting enzyme 2 (ACE2) on lung cells, decreasing therefore their susceptibility to the virus.<sup>11</sup> Similar to TMPRSS2, ACE2 expression has also been shown to be regulated by the AR.<sup>12</sup>

The androgen regulation of TMPRSS2 and ACE2 raises the possibility that antiandrogens may inhibit the cell entry of other coronaviruses, which either enter target cells via a TMPRSS2-dependent pathway and/or use ACE2 as their cell receptor. Several cell receptors have been described for HCoV, including aminopeptidase N for 229E,<sup>13</sup> and ACE2 for NL63.<sup>14</sup> The cellular receptors for OC43 and the uncultivable in cell

culture HKU1 are currently unknown, but O-acetylated sialic acids, Kallikrein 13 and TMPRSS2 have been identified as important cell entry factors.<sup>15,16</sup> Following binding to cell receptors, HCoV, like most coronaviruses, gain access to the cells either via direct fusion with the cell membrane or via cathepsin-mediated endocytosis.<sup>17</sup> Several studies reported that circulating OC43, HKU1, and 229E HCoV generally use cell-surface TMPRSS2 for cell entry and not endosomal cathepsins in human airway epithelial cells.<sup>18–20</sup> It was suggested that NL63 preferentially enters target cells through the endocytic route, but it can employ TMPRSS2 and bypass endocytosis in airway epithelial cells.<sup>21</sup>

In this study, we aimed to investigate the significance of TMPRSS2 in facilitating cell entry of NL63 and 229E viruses in A549 immortalized human lung cells and evaluate the potential of the antiandrogen enzalutamide to inhibit virus entry. We observed reduced susceptibility to pseudotypes expressing the spike glycoproteins of NL63 and 229E viruses and wild-type NL63 and 229E viruses in enzalutamide-treated A549 human lung epithelial cells overexpressing ACE2. However, this effect was not observed for the OC43 wild-type virus. Collectively, our data suggest that antiandrogens are promising candidates for the development of broad-spectrum therapeutics to treat a range of coronaviruses.

## 2 | MATERIALS AND METHODS

### 2.1 | Plasmids, cell lines, and inhibitors

The HCoV-229E and -NL63 seasonal S genes were synthesized and inserted into a pcDNA3.1<sup>+</sup> backbone by GeneArt Gene Synthesis, Thermo Fisher. The human ACE2 receptor plasmid pCAGGS-ACE2 and the human TMPRSS2 protease encoding pCAGGS-TMPRSS2 plasmid were provided by S. Pöhlmann and M. Hoffman from the German Primate Center (Leibniz Institute for Primate Research). The lentiviral packaging plasmid p8.91 and firefly luciferase reporter plasmid pCSFLW were used for pseudotype production as previously described.<sup>22</sup>

Human embryonic kidney (HEK293T/17), human epithelial colorectal adenocarcinoma (Caco-2; ATCC:HTB-37), human fetal lung fibroblast-like (MRC-5; ATCC:HTB-37), monkey epithelial kidney cells (LLC-MK2; ATCC:CCL7), mink epithelial lung cells (Mv1Lu; ATCC:CCL64), and human adenocarcinoma alveolar basal epithelial (A549; ATCC: CRM-CCL-185) cells were maintained using Dulbecco's Modified Eagle Medium (DMEM; GIBCO BRL) supplemented with 10% fetal bovine serum (FBS; Invitrogen) and 1% penicillin/streptomycin (P/S; Sigma). A549 clone 8 cells stably expressing ACE2 alone or ACE2 and TMPRSS2 were purchased from NIBSC (reference-codes: 101005 and 101006) and maintained as previously described.<sup>23</sup> All cell lines were grown at 37°C and in a humidified atmosphere of 5% CO<sub>2</sub>.

### 2.2 | Pseudotype virus production

Pseudotypes expressing the spike glycoproteins of NL63, 229E, SARS-CoV-2, VSV (vesicular stomatitis virus)-G or no ( $\Delta$ -env) glycoprotein were

produced as described.<sup>24</sup> Briefly, the lentiviral packaging plasmid p8.91, the pCSFLW firefly luciferase vector, the pcDNA3.1<sup>+</sup> expression plasmids for spike proteins were co-transfected using Fugene HD (Promega) into HEK293T/17 cells. Filtered supernatants were collected 48–72 h post-transfection. Two-fold serial dilutions of PV-containing supernatant were performed as previously described using 96-well plates.<sup>22</sup> Briefly, plates were incubated for 24–48 h, after which 50  $\mu$ L Bright-Glo substrate (Promega) was added. Luciferase readings were conducted with a luminometer (GLOMAX<sup>™</sup>, Promega) after a 5-min incubation. Data were normalized using  $\Delta$ -env and cell-only measurements and expressed as relative luminescence units (RLU) per mL.

### 2.3 | Virus infections, enzalutamide treatment, and virus titration

All work involving the use of viruses was performed within BSL-2 laboratory under Health and Safety guidelines of the University of Essex. The HCoV-NL63 reference strain (isolate Amsterdam 1 [Ams-001]) was a kind gift from Dr. Lia van der Hoek and the OC43 and 229E strains were obtained from ATCC (VR-1558<sup>™</sup> and VR-740<sup>™</sup> respectively). The viruses were propagated in LLC-MK2, Mv1Lu and MRC-5 cells respectively. For antiandrogen treatment, cells were pretreated with enzalutamide (ENZA, Stratech Scientific Ltd; 1  $\mu$ g/mL) 48–72 h before infection. For infection assays, MRC-5 or Caco-2 cells were seeded in 12-well plates and incubated at 37°C with 5% CO<sub>2</sub>, until they reached 80% confluency. Unless otherwise specified, cells were infected for 2 h with 229E, OC43 and NL63 respectively at a multiplicity of infection (MOI: 1). Media were then removed and replaced with DMEM and 2% heat-inactivated FBS, 1% P/S at 33°C for 2 days. The viruses released into the supernatant were then harvested and quantified by calculation of a 50% tissue culture infective dose per mL (TCID<sub>50</sub>/mL) according to the Reed–Muench formula and qPCR. Camostat mesylate (TMPRSS2 inhibitor) and E-64d (endosomal protease inhibitor) were obtained from MilliporeSigma. dose–response curve analyses were conducted for remdesivir (GS-5734<sup>™</sup>, Gilead Sciences, Inc) and enzalutamide. Stock solutions of remdesivir and enzalutamide, each at a concentration of 10 mM, were prepared in dimethyl sulfoxide (DMSO). MRC-5 cells underwent pretreatment with varying concentrations of enzalutamide for 3 days, with remdesivir for 2 h, or pretreated with equivalent volumes of DMSO (mock) before continuous 96 h infection (33°C) with 229E or OC43 at MOI:0.01. The determination of the 50% effective concentration (EC<sub>50</sub>) and 50% cytotoxic concentration (CC<sub>50</sub>) followed previously established methods,<sup>25</sup> and was conducted using GraphPad Prism 10.2.0 (GraphPad Software) employing the nonlinear regression fit model.

### 2.4 | Real-time quantitative reverse transcription PCR (qRT-PCR)

All qRT-PCR analyses were conducted using the CFX96 Real-time PCR system (Biorad). Viral RNA from the cell supernatant was extracted with TRIzol<sup>™</sup> Reagent (Fisher Scientific) as per the

manufacturer instructions. For OC43, NL63, and 229E nucleocapsid (N) gene PCR detection, a standard curve was generated using RNA dilutions of known copy number (ATCC standards: VR-1558DQ, VR-3263SD, VR-740DQ respectively) to allow absolute quantification of N copies from C<sub>t</sub> values as previously described.<sup>26</sup> Cell RNA isolation and RT-qPCR were performed using the PowerUp<sup>™</sup> SYBR Green Master Mix (Fisher Scientific), following previously published procedures.<sup>27,28</sup> Primer sequences for GAPDH, ACE2, TMPRSS2, Cathepsin-B, and Cathepsin-L were obtained from the literature.<sup>9,29</sup> The quantitative gene expression data were normalized to the housekeeping gene GAPDH and compared with mock controls using plasmids containing the target genes as standards. Expression levels were quantified as gene copies per 1  $\mu$ g RNA. All samples were tested in triplicate to ensure reproducibility.

### 2.5 | RNA-sequencing of nasal airway epithelial cells infected with HCoV

Air–liquid interface human nasal airway epithelial cells (HAE, MucilAir<sup>™</sup>; pool of 14 donors, catalog no. EP02MP; age and gender of donors are listed in Supporting Information S1: Material 1) were purchased from Epithelix and maintained in Mucilair cell culture medium (Epithelix). HAE were kept at 5% CO<sub>2</sub>, 37°C. Briefly, before infection HAE were washed with serum-free media to remove mucus and debris. Cells were infected with 200  $\mu$ L of virus-containing (HCoV-229E and -OC43) serum-free DMEM (MOI: 0.01) and incubated at 33°C for 1 h. Inoculum was then removed, and cells were washed twice. Time points were taken by adding 200  $\mu$ L of serum-free DMEM and incubating for 10 min and 37°C before removal and titration.

The cells were harvested at 24 and 72 h for RNA isolation using the RNeasy Mini Plus kit (Qiagen). Approximately 1  $\mu$ g of RNA was used for the construction of sequencing libraries. The mRNA library preparation (poly-A enrichment) and sequencing were performed by Novogene.<sup>30</sup> The sequencing data (FASTQ raw files) were imported into Partek Flow (version 10.0, build 10.0.23.0531; Partek Inc.) for quality control and further processing. Paired-end reads were trimmed based on the Phred quality score threshold of >20 and aligned to the human genome (hg38) using the STAR-2.7.8a aligner. Quantification of gene expression was performed using the transcript model Ensembl Transcripts release 104 v2, and the data were subsequently normalized by the counts per million (CPM) method.<sup>30</sup> Differential expressed genes were identified using the DESeq2 package. Genes were considered differentially expressed if they met the following criteria:  $p < 0.05$ , false discovery rate (FDR) < 0.05, and a fold change  $\geq 2$  or  $\leq -2$ .

### 2.6 | Luciferase assay

MRC-5 cells were seeded at  $1 \times 10^4$  cells/well in hormone-depleted DMEM media (phenol-red free media containing 5% charcoal stripped FCS, 1% penicillin streptomycin) in 96-well plates. After 24 h, cells were

co-transfected with TAT-GRE-EIB-LUC (500 ng/ $\mu$ L), pSVAR (100 ng/ $\mu$ L), and pRV-renilla (100 ng/ $\mu$ L) using FuGENE HD transfection reagent as before.<sup>31</sup> At 48 h posttransfection, cells were treated  $\pm$ 1 nM Mibolerone, and/or infected with OC43 or 229E (MOI 1) for 2 h and lysed at 96 h using 25  $\mu$ L Dual-Glo<sup>®</sup> Luciferase Assay System (Promega). Luminescence was measured, and renilla luminescence was used for normalization with FLUOstar<sup>™</sup> Omega plate reader (BMG Labtech).

## 2.7 | Phylogenetic analysis

The amino acid sequences of coronavirus spike orthologues were subjected to multiple alignment using CLC Workbench 7 (CLC Bio; Qiagen). Protein sequence NCBI reference sequences for the indicated viruses are as follows: SARS-CoV-2 (YP\_009724390.1), 229E (QNT54842.1), NL63 (ANU06084.1), OC43 (CAA83660.1), and HKU1 (UJH59888.1).

## 2.8 | Data analyses

All analyses and graphs were performed using GraphPad Prism software version 10.2.0 (GraphPad) and R, version 4.0.3 (R Foundation for Statistical computing). UpSet plots were generated using the R package UpSetR v1.4.0 and heat maps were generated using the Broad Institute's Morpheus software (<https://software.broadinstitute.org/morpheus/>). The single-cell RNA sequencing data set PRJNA789548 was re-processed, examined, and visualised using Cellenics<sup>™</sup> community instance (<https://scp.biomage.net/>) hosted by Biomage (<https://biomage.net/>). All data are presented as means with standard deviation (SD). Statistical analysis was carried out where appropriate to determine whether data were significant. Shapiro-Wilk normality tests were performed and based on the results we performed one/two-way ANOVA tests with Tukey's multiple comparison tests.  $p < 0.05$  was considered significant unless otherwise stated.

## 2.9 | Data access

New high-throughput data generated in this study have been submitted to the NCBI Gene Expression Omnibus (GEO) (<http://www.ncbi.nlm.nih.gov/geo/>) under accession number GSE238079.

## 3 | RESULTS

### 3.1 | Overexpression of TMPRSS2 facilitates cell entry of NL63 and 229E pseudotypes in A549 cells expressing ACE2 and TMPRSS2

The alignment of amino acid sequences of the spike protein in both seasonal coronaviruses (HCoV) and SARS-CoV-2 show a significant level of homology conservation at the S2' TMPRSS2 cleavage site

(Figure 1A). To examine the functional significance of TMPRSS2 in the cell entry of HCoV, we employed the A549 cell line, derived from human lung adenocarcinoma, which is known to be androgen responsive.<sup>32</sup> A549 cells express low constitutive levels of ACE2 and TMPRSS2 and thus are poorly permissive to infection by NL63, SARS-CoV-2 or spike pseudotyped lentiviral particles of HCoV and SARS-CoV-2 (in-house data).<sup>23</sup> For our study, we used two sublines of A549 cells stably transfected to ectopically express either ACE2 alone (A549<sup>ACE2</sup>) or both ACE2 and TMPRSS2 (A549<sup>ACE2S2</sup>).<sup>23</sup> To investigate NL63 and 229E virus cell entry, we generated lentivirus pseudotypes (PV) incorporating their respective spike glycoproteins (Figure 1B). OC43 lentiviruses consistently exhibited low levels in various cell lines, including HEK293T and Huh7.5 cells, irrespective of the expression of OC43 spike and/or membrane proteins (Figure 1C) and/or esterase protein (data not shown). Consequently, they were excluded from subsequent analyses.

PV bearing SARS-CoV-2 S- and Vesicular stomatitis virus G-glycoproteins (VSV-G) served as positive controls and PV without envelope protein ( $\Delta$ -env) served as negative controls. A549, A549<sup>ACE2</sup>, and A549<sup>ACE2S2</sup> were transduced with the respective PV for 48 h and viral entry was assayed via the expression of a PV-encoded luciferase reporter. Our data (Figure 1B) show that A549 were not susceptible to NL63- and SARS-CoV-2-PV but were susceptible to VSV-G-PV and marginally susceptible to 229E-PV. A549<sup>ACE2</sup> were more susceptible to NL63- and SARS-CoV-2-PV (by 30 and 140-fold transduction increase respectively) compared to wild type A549 as expected since ACE2 is the entry receptor for both NL63 and SARS-CoV-2.<sup>14</sup> Upon addition of ectopic TMPRSS2, A549<sup>ACE2S2</sup> were more susceptible to all three PV compared to A549 (>80-fold for each of them) suggesting that elevated levels of TMPRSS2 enhance cell entry of all of the viruses investigated, in line with published work.<sup>33</sup>

### 3.2 | Inhibition of TMPRSS2 by camostat mesylate reduces cell entry of NL63- and 229E-pseudotypes

To further investigate the significance of TMPRSS2 in the cell entry of HCoV, we treated A549<sup>ACE2S2</sup> cells before PV transduction with the drugs camostat and E64-d, which are known to inhibit the activity of TMPRSS2 and cathepsin-L, respectively. Our results (Figure 2A) indicate that the TMPRSS2-inhibitor camostat reduced the entry of NL63, 229E, and SARS-CoV-2 PV by 74%, 61%, and 72%, respectively. On the other hand, E64-d reduced the entry of NL63 PV by 21%, 229E by 55%, and SARS-CoV-2 by 29%. When both E64-d and camostat were combined, we observed a further reduction in the entry of NL63, 229E, and SARS-CoV-2 by 87%, 68%, and 82%, respectively. Entry of the positive control PV, VSV-G, did not show any significant reduction. The results suggest that A549<sup>ACE2S2</sup> cells have an operational TMPRSS2-dependent pathway for the entry of NL63, 229E, and SARS-CoV-2 PV. The combined use of camostat and E64-d resulted in a more substantial reduction in viral entry, indicating possible roles of both TMPRSS2 and cathepsin-L in facilitating the entry of these viruses. The smaller reduction in entry observed after treatment with

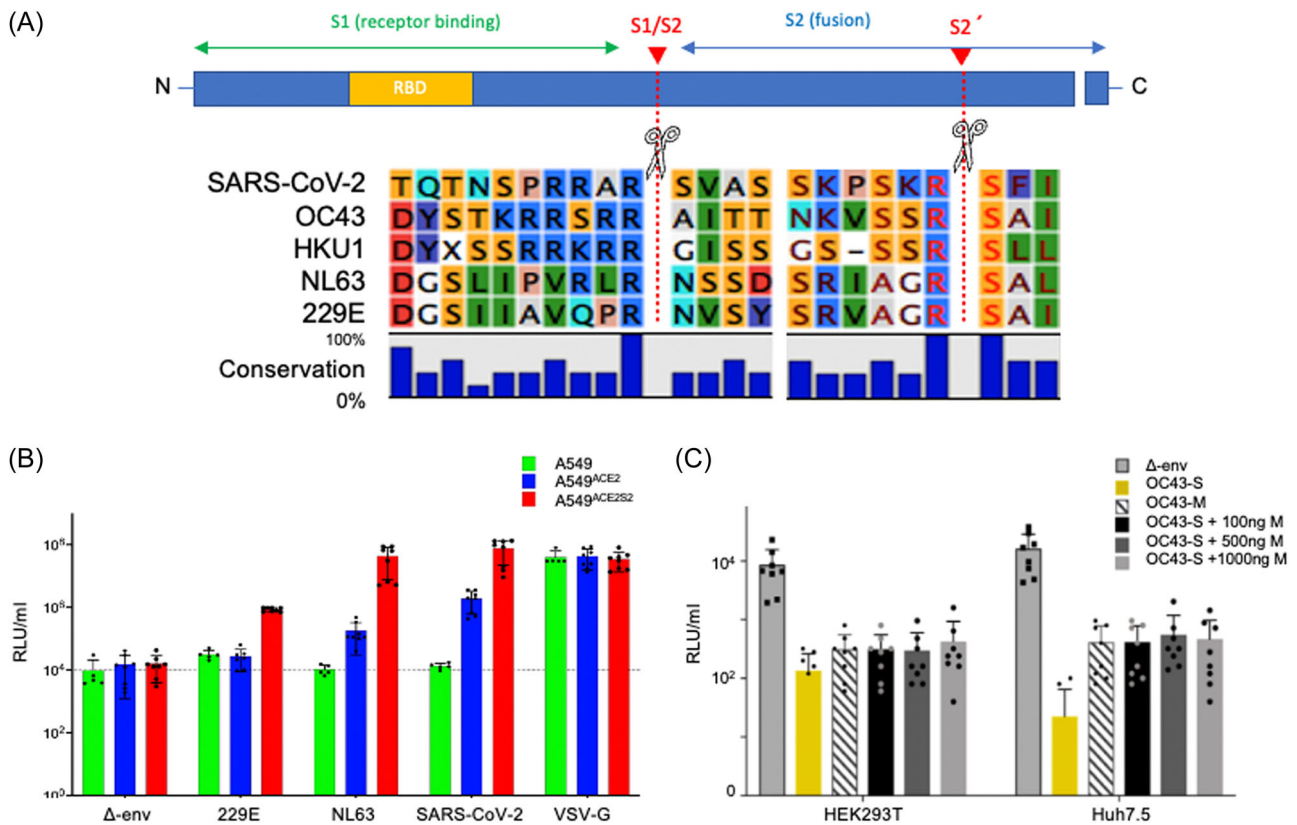


**FIGURE 1** (A) Amino acid sequence alignment of S proteins from various human coronaviruses (HCoV) and SARS-CoV-2 at the S1/S2 and S2' cleavage site. The receptor binding domain (RBD), spike glycoprotein subunits (S1 and S2), and S1/S2 and S2' cleavage sites are labeled. Multiple amino acid sequence alignment was performed by CLC Workbench (CLC Bio/Qiagen). The RasMol color scheme was used, where amino acids are colored according to traditional amino acid properties. Amino acids associated with the outer surface of a protein are given bright colors and nonpolar residues are darker. (B) Transduction efficiencies (mean  $\pm$  SEM,  $n = 8$ ) of  $\Delta$ -env, NL63, 229E, SARS-CoV-2 S, and VSV-G pseudoviruses in A549, A549<sup>ACE2</sup>, and A549<sup>ACE2S2</sup> cells at 48 h posttransduction, as measured by luciferase activity and expressed as relative luminescence units (RLU/ml). (C) The figure depicts the susceptibility of HEK293T and Huh7.5 cells to OC43 pseudovirus (PV) expressing or lacking the spike (S) glycoprotein or transfected with varying levels of membrane (M) protein expression plasmid ( $n = 8$ ). Data are presented as average means, with error bars indicating standard deviation (SD). Statistical significance was determined by one-way ANOVA and Tukey's post hoc tests compared to untreated control (\* $p = 0.05$ , \*\* $p = 0.005$ , \*\*\* $p = 0.0005$ , \*\*\*\* $p < 0.0001$ ).

E64-d alone suggests that cathepsin-L may play a less significant role in the entry of these viruses compared to TMPRSS2 in these cell lines.

### 3.3 | Enzalutamide reduces cell entry of 229E and NL63-PV in A549<sup>ACE2</sup> and A549<sup>ACE2S2</sup> cells

To investigate the role of enzalutamide (ENZA) in inhibiting cell entry of NL63 (Figure 2B), 229E, and SARS-CoV-2, we used PV to transduce A549<sup>ACE2</sup> and A549<sup>ACE2S2</sup> cells, which were pretreated with enzalutamide for 72 h. In A549<sup>ACE2</sup> cells, enzalutamide significantly reduced viral entry of NL63, 229E, and SARS-CoV-2 PV by approximately 74%, 85%, and 50%, respectively (Figure 2C). To evaluate the potential influence of hormone levels on the observed outcomes, the experiments were replicated using hormone-depleted (charcoal stripped) media, yielding consistent results (Figure 2D).

To further explore the contribution of TMPRSS2 in viral entry, we conducted an experiment using A549<sup>ACE2S2</sup> cells. In these cells, the

expression of exogenous ACE2 and TMPRSS2 were insensitive to androgen signaling, as the genes are under the control of the non-androgen responsive EF1a promoter.<sup>23</sup> The results showed that enzalutamide partially reduced cell entry by approximately 60%, 55%, and 31% for NL63, 229E, and SARS-CoV-2, respectively. This suggests that when TMPRSS2 expression is regulated independently of androgen receptor, the effect of enzalutamide is attenuated but not eliminated. Furthermore, as expected enzalutamide did not impact the entry of VSV-G PV, indicating that enzalutamide's effect is specific to HCoV and SARS-CoV-2 entry mechanisms.

### 3.4 | Enzalutamide reduces replication of authentic 229E and NL63, but not OC43, in both TMPRSS2-expressing and nonexpressing cells

To confirm the results obtained with pseudotyped viruses, we quantified viral particle levels in the supernatant of Caco-2 and

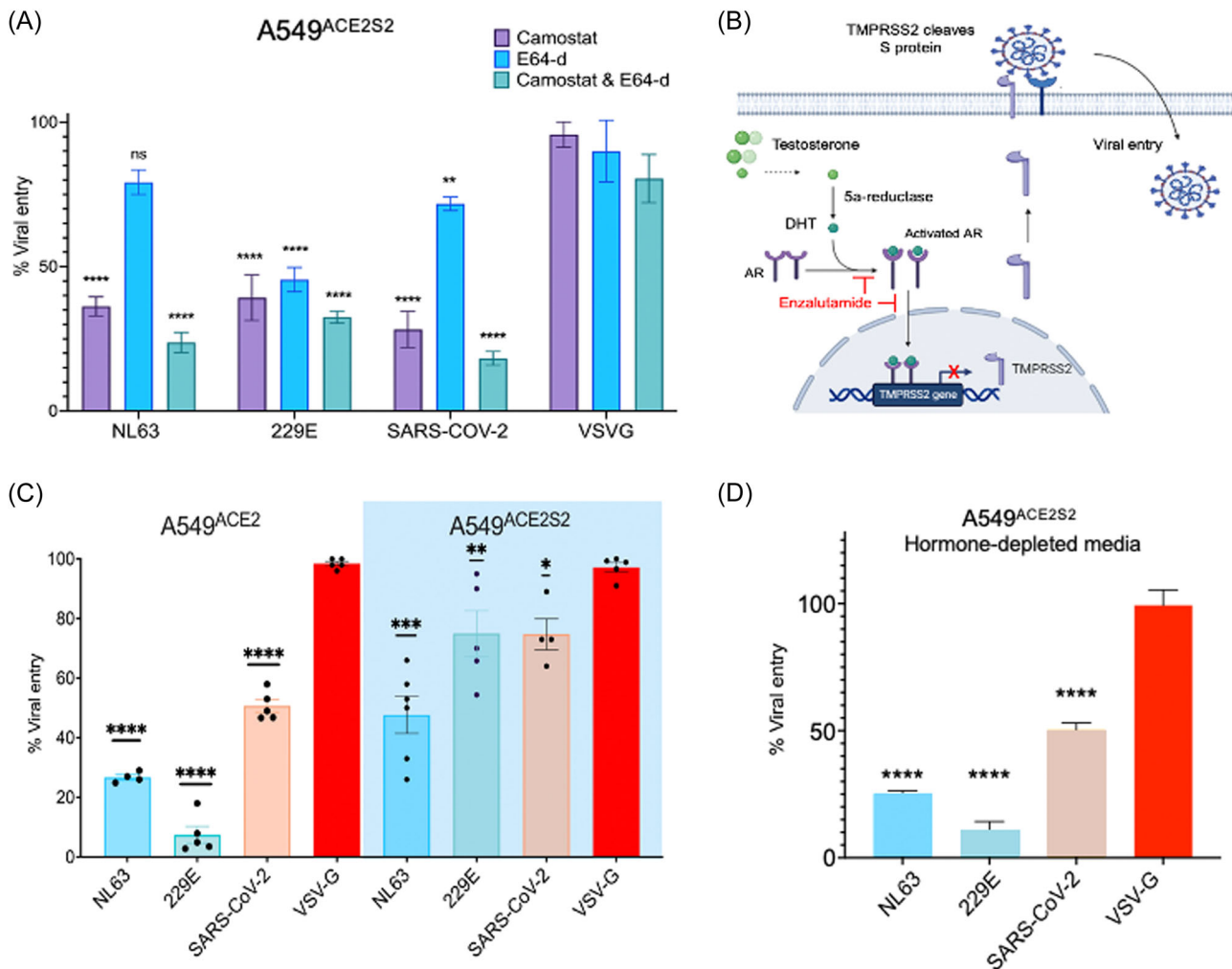


**FIGURE 2** (A) Percent pseudovirus (PV) transduction levels (mean  $\pm$  SEM,  $n = 3$ ) in A549<sup>ACE2S2</sup> cells pretreated with camostat (50  $\mu$ M) and/or E64-D (25  $\mu$ M) inhibitors. Statistical significance was determined by two-way ANOVA and Tukey's post hoc tests compared to untreated control (\*\* $p = 0.005$ , \*\*\*\* $p < 0.0005$ , ns: not significant). (B) Androgen receptor signaling and how antiandrogen therapies might block viral uptake. In the absence of androgen, the AR is located in the cytoplasm. Ligand binding promotes dissociation of this complex, nuclear localization and dimerization. The AR binds to androgen response elements in the regulatory regions of target genes (e.g., TMPRSS2) and regulates their transcription. Enzalutamide binds to and inhibits the AR. The downregulation of AR signaling may reduce TMPRSS2 expression, reducing in-turn TMPRSS2-dependent viral entry. The schematic was created with BioRender.com. (C) Percent PV transduction levels (mean  $\pm$  SEM,  $n = 6$ ) in A549<sup>ACE2</sup> and A549<sup>ACE2S2</sup> cells pretreated with enzalutamide (1  $\mu$ g/mL) for 72 h. Statistical significance was determined by one-way ANOVA and Tukey's post hoc tests compared to untreated control (\* $p = 0.05$ , \*\* $p = 0.005$ , \*\*\* $p = 0.0005$ , \*\*\*\* $p < 0.0001$ ). (D) Percent PV transduction levels (mean  $\pm$  SEM,  $n = 6$ ) in A549<sup>ACE2</sup> cells grown in charcoal-stripped serum and pretreated with enzalutamide (1  $\mu$ g/mL) for 72 h. Statistical significance was determined by one-way ANOVA and Tukey's post hoc tests (\*\*\*\* $p < 0.0001$ ).

MRC-5 cells following 72 h of enzalutamide treatment (1  $\mu$ g/mL) and subsequent infection with authentic 229E, OC43, and NL63 viruses, respectively (Figure 3A). Additionally, we examined the mRNA expression of key proteases in the utilized cell lines, as depicted in Figure 3B. We observed a significant reduction in viral copies from  $2.79 \times 10^7$  to  $7.4 \times 10^6$  for NL63 and from  $3.54 \times 10^6$  to  $5.8 \times 10^5$  for 229E, further confirming the inhibitory effect of enzalutamide on the entry of these viruses (Figure 3A). Interestingly, enzalutamide did not significantly affect the cell entry of OC43.

To investigate the mechanism of action of enzalutamide, we assessed the mRNA expression levels of ACE2 and proteases involved in the cellular entry of coronaviruses by RT-qPCR (Figure 3B). Our findings demonstrate that NL63-permissive Caco-2 cells express TMPRSS2, TMPRSS4, and ACE2, while 229E- and OC43-permissive MRC-5 cells exhibit no constitutive expression of TMPRSS2, TMPRSS4, and ACE2. In contrast, A549 cells required lentiviral transduction to establish stable ACE2 and TMPRSS2 expression, to render them susceptible to 229E/NL63 and SARS-CoV-2 pseudoviruses. Conversely, nonandrogen responsive cathepsins B and L

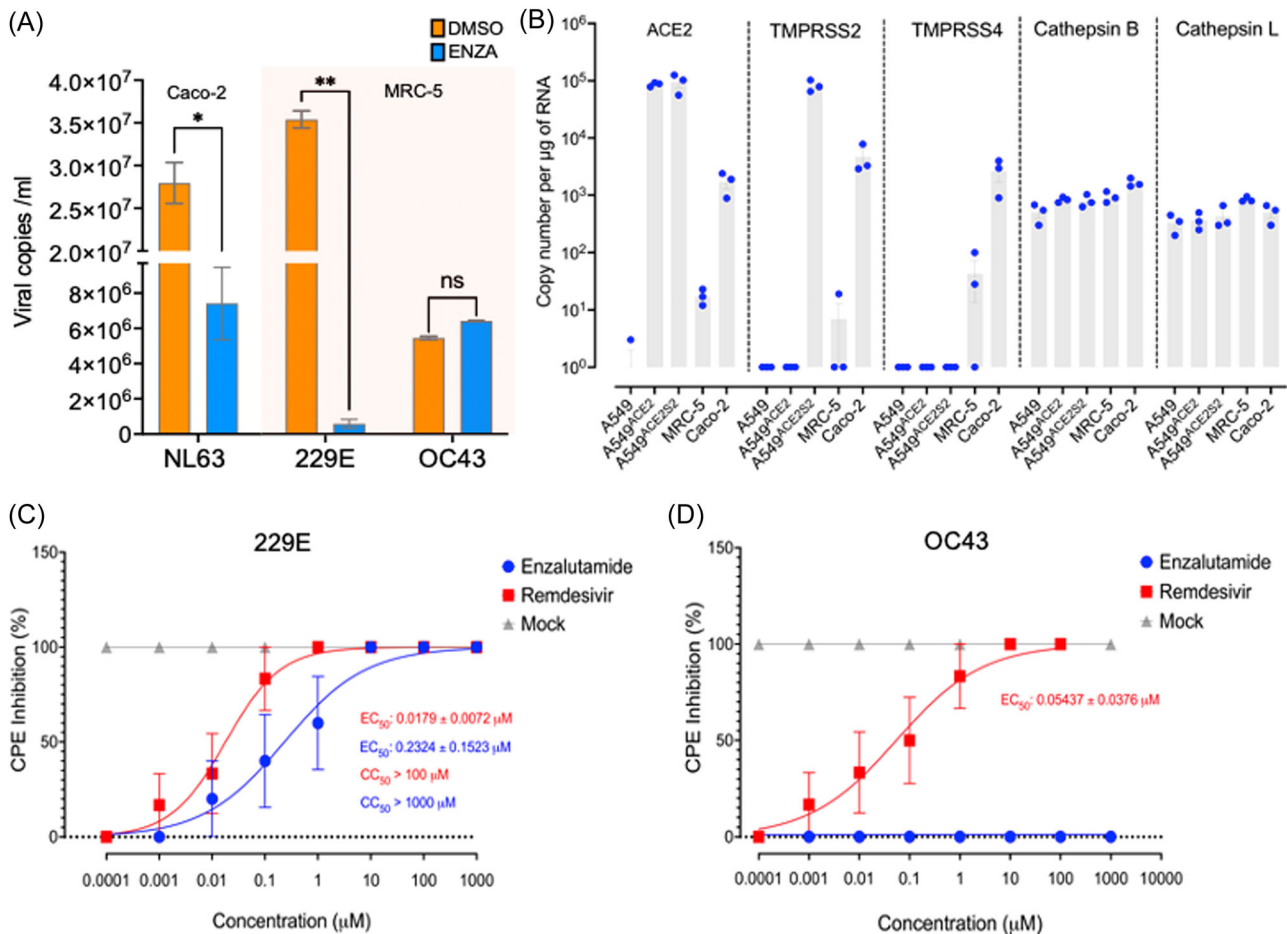


**FIGURE 3** (A) Quantification of viral RNA copies in cell culture supernatant after pretreatment of MRC-5 and Caco-2 cells with enzalutamide (1 µg/mL) for 72 h and infection with 229E and NL63 viruses (MOI: 1), respectively, as determined by qRT-PCR for the nucleocapsid (N) gene. DMSO-treated cells were used as controls in each cell line. Analysis was performed in two independent experiments. Statistical significance was determined by two-way ANOVA and Šidák's post hoc tests (\* $p = 0.05$ ). (B) Quantification of ACE2 and proteases (TMPRSS2, TMPRSS4, Cathepsin B and L) copy numbers per µg of total cellular RNA in the examined cell lines was carried out using qRT-PCR analysis, with plasmids serving as reference standards for precise calculation. (C and D) Dose–response curve analyses, indicating the percentage of cytopathic effect (CPE) inhibition, were performed in MRC-5 cells infected with 229E (C) and OC43 (D) at a multiplicity of infection (MOI) of 0.01 for 96 h. The blue line represents various concentrations of enzalutamide, the red line shows remdesivir (positive control), and the gray line illustrates Mock-stimulated cells treated with equivalent volumes of DMSO as a negative control. The data, depicting the mean ( $\pm$ SEM) of at least two independent experiments conducted in duplicate, include EC<sub>50</sub> (50% effective concentration) or CC<sub>50</sub> values (50% cytotoxic concentrations) indicated in the graphs.

exhibited constitutive expression across all tested cell lines. Taken together these results suggest that enzalutamide may also exert its effect via non-TMPRSS2-mediated mechanisms that inhibit viral entry and possibly replication.

To confirm the differential impact of enzalutamide on 229E and OC43, we then performed dose–response curve analyses to determine EC<sub>50</sub> values (EC<sub>50</sub>, half-maximal effective concentration) in MRC-5 cells. The calculated EC<sub>50</sub> for 229E was 0.2324 µM, signifying the concentration at which enzalutamide exerts a half-maximal inhibitory effect on this virus. Notably, OC43 exhibited no cytopathic effect (CPE) inhibition at any tested concentration. As a positive control, remdesivir demonstrated an EC<sub>50</sub> of 0.0179 µM for 229E and 0.05437 µM for OC43 (Figure 3C,D).

### 3.5 | Distinct androgen signaling responses to HCoV infections in primary human nasal airway cells

In the context of our investigation, we aimed to assess the influence of HCoV on AR activity and signaling, providing insights into the varied effects of enzalutamide across different HCoV. To achieve this, we conducted RNA-sequencing analysis (RNA-seq) on CoV-target cells namely air-liquid interface nasal epithelial cells (HAE) infected with two distinct strains: 229E, belonging to the alpha lineage and OC43, representing the beta lineage. Our choice to study both strains was deliberate; enzalutamide demonstrated efficacy against 229E but not OC43 (Figure 3A), prompting a more focused exploration of these viruses. The HAE cells were derived from a pool

of 14 human donors (Supporting Information S1: Material 1), ensuring representation of both genders in the study. These primary cells faithfully replicate normal airway biology, featuring pseudostratified mucociliated differentiation and organotypic cell types.<sup>34</sup>

Our primary objective was to determine enrichment patterns between gene sets influenced by the viruses and genes known to be responsive to androgen signaling. By employing three established androgen-responsive gene signatures,<sup>35-37</sup> we examined changes in AR activity prompted by HCoV, specifically focusing on the comparisons between virus-infected and uninfected cells. The gene signatures included the androgen-induced geneset in MD-SB1 breast cancer cells,<sup>38</sup> the androgen-induced geneset in LNCaP cells<sup>39</sup> and the hallmark androgen response geneset M5908 (mSiGdb).<sup>40</sup> The results, depicted in Figure 4A,B, revealed significant differences in how AR-regulated genes responded to the two viruses. Specifically, 229E induced changes in a subset of AR-regulated transcripts (22 and 135 at 24 and 72 h postinfection, respectively, out of 185 assessed), whereas OC43 affected only a limited number of such transcripts (8 and 21 at 24 and 72 h, respectively, out of 185 assessed; Figure 4A,B). The complete data set of androgen-responsive gene expression can be found in Supporting Information S1: Material 2.

As we saw changes in AR target gene expression, we were interested to see if AR levels were altered in response to the HCoV. However, our attempts to detect alterations in AR levels through RNA-seq reads and immunoblotting, in response to viral infection, yielded inconclusive results, likely due to low detection sensitivity and cellular heterogeneity (data not shown). This led us to hypothesize that AR might still be active, albeit with restricted expression in specific nasal airway cell types. To gain further insights, we reanalyzed publicly available single-cell RNA-seq data of HAE, revealing AR expression is relatively enriched in epithelial and airway goblet cells compared to other nasal epithelial cell types (Figure 4C). Together, these findings suggest a significant influence of 229E on global androgen signaling even in primary cells with low AR expression.

To investigate whether the elevated expression of the androgen-induced core genes can be attributed to a direct effect of the virus on the androgen receptor, we employed a luciferase reporter under the control of an ARE (Figure 4D). MRC-5 cells, which exhibit low androgen receptor expression, maintained in androgen-depleted media, and mock-infected or infected with 229E or OC43 viruses. Simultaneously, they were co-transfected with an AR expression vector and an ARE-luciferase reporter, with or without stimulation with the synthetic androgen mibolerone. MRC-5 cells infected with 229E exhibited a significant increase in luciferase activity both in the presence and absence of mibolerone compared to mock-infected cells, suggesting ligand-dependent activation of the AR by the virus. In contrast, OC43 infection resulted in no luciferase activity in the absence of mibolerone and suppressed stimulation of the AR when activated by mibolerone.

## 4 | DISCUSSION

Seasonal coronaviruses (HCoV) pose a significant public health burden, yet they remain relatively neglected compared to other coronaviruses.<sup>2</sup> This is evident from the lack of specific vaccines or drugs and the incomplete global understanding of their epidemiology, largely due to their exclusion from standard diagnostics.<sup>2,41,42</sup> Certain drugs originally developed for other viral infections, such as interferons, ribavirin, and mycophenolic acid, have demonstrated promising outcomes against HCoV in clinical trials.<sup>43</sup> In this study, our attention turned to enzalutamide, a nonsteroidal antiandrogen drug employed in the treatment of prostate cancer,<sup>44</sup> which we previously demonstrated to inhibit SARS-CoV-2 infection in lung cells.<sup>9</sup> We report here that enzalutamide effectively reduces 229E and NL63 entry and infection in immortalized lung cells, but no discernible effect was observed against OC43.

Enzalutamide functions by binding to and inhibiting the transcriptional activity of the androgen receptor (AR), a ligand-dependent transcription factor and its protein drug target.<sup>44</sup> This inhibition attenuates the activation of genes regulated by AR, which is not only expressed in the prostate but also various other tissues including the lungs.<sup>32</sup> Additionally, enzalutamide has been shown to down-regulate TMPRSS2 expression, an AR-upregulated type II transmembrane serine protease that cleaves the spike protein of SARS-CoV-2, preventing the virus from entering lung cells.<sup>9</sup> This mechanism of action suggests the potential of enzalutamide as a treatment option for other viruses that rely on TMPRSS2 for cell entry.

In this study, we explored the involvement of TMPRSS2 in the enzalutamide mechanism of action against HCoV. Employing pseudotyped viruses, we observed a significant inhibitory effect of enzalutamide on the entry of 229E and NL63 in cells overexpressing TMPRSS2, underscoring its importance as a key entry factor for HCoV, including NL63, whose cell entry is not considered TMPRSS2-dependent.<sup>21</sup> Elevated TMPRSS2 levels in cells with typically low expression may alter the infection dynamics, potentially bypassing the endocytic, cathepsin-dependent pathway commonly employed by viruses like NL63.<sup>21,45</sup> This suggests that enzalutamide most likely exerts its antiviral effects by influencing TMPRSS2 activity. However, we also noted that enzalutamide exerts an effect in cells lacking TMPRSS2 expression. Consequently, the influence of enzalutamide on androgen signaling via TMPRSS2 regulation cannot be considered the sole factor contributing to its observed effects, implying additional mechanisms of action. The drug's efficacy may be associated with various androgen-responsive factors, including neuropilin-1, furin, TMPRSS4, and cathepsin G, pivotal in cell entry<sup>35-37</sup> or other essential processes for coronavirus replication. Moreover, the observed antiviral impact might be influenced by off-target effects, distinct from its primary role as an androgen receptor inhibitor.

The interaction between viruses and host cells plays a pivotal role in regulating essential molecular pathways, including those linked to immune response, cell survival, proliferation, and gene expression. Previous studies have demonstrated that viruses can act as noncellular positive coregulators for androgen receptor (AR).<sup>36,46,47</sup>



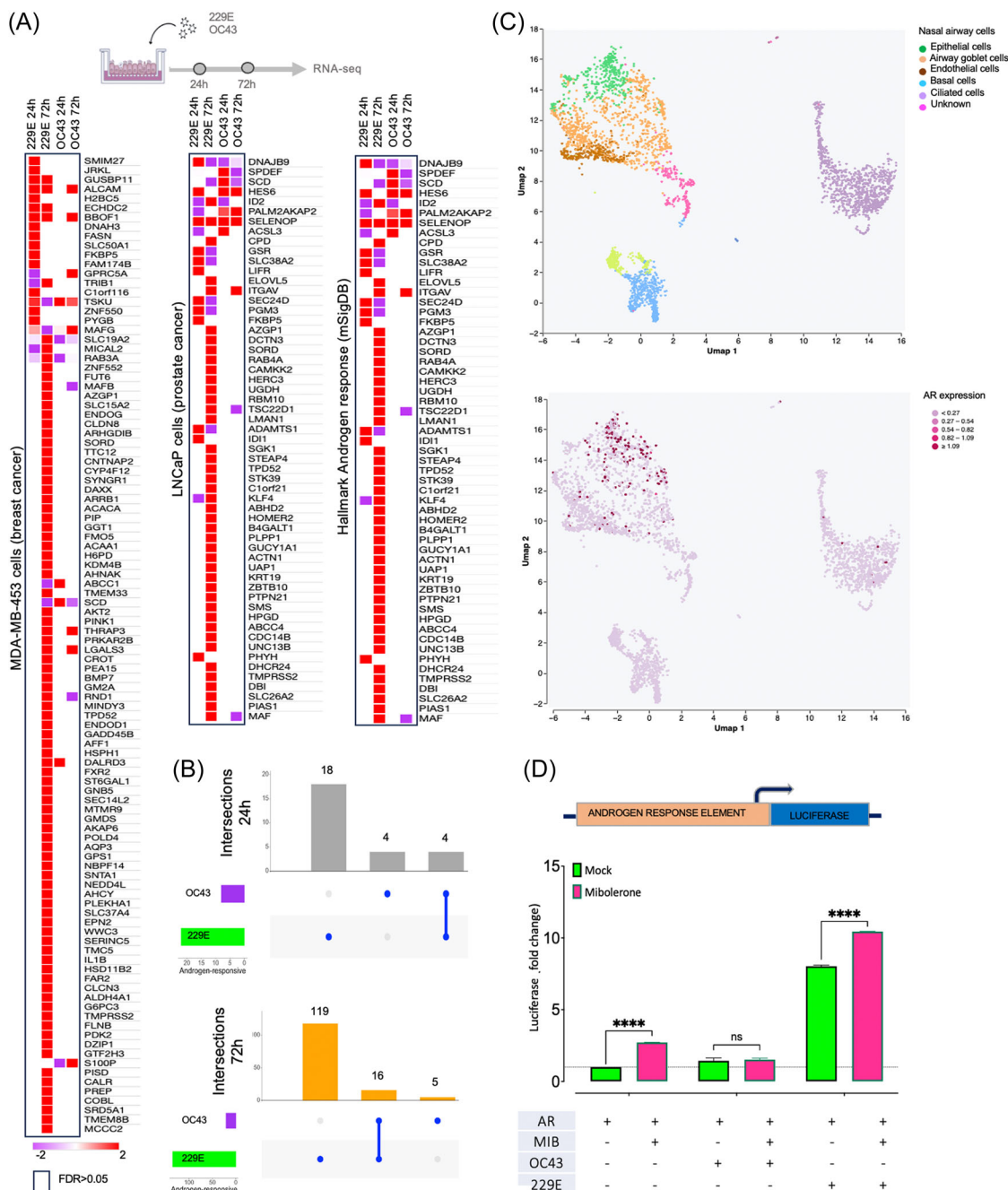


**FIGURE 4** Distinct androgen signaling responses to viral infections: (A) Primary human nasal airway cells were infected with human coronaviruses OC43 and 229E, and the differential gene expression analysis at 24 and 72 h postinfection was performed using bulk RNA-sequencing. The heat maps illustrate the relative transcript expression of genes previously recognized as androgen-responsive in three published datasets, examining their expression under virus-infected versus uninfected conditions. These data sets comprise: androgen-induced geneset in MD-SB1 breast cancer cells,<sup>38</sup> androgen-induced geneset in LNCaP cells<sup>39</sup> and the hallmark androgen response geneset M5908 (mSiGdb).<sup>40</sup> (B) Upset plots visually present the intersection of androgen-responsive transcripts differentially regulated by 229E and OC43 viruses (virus-infected vs. uninfected) at two critical time points—24 h (upper panel) and 72 h (lower panel) postinfection. The colored bar plots (left) show the number of androgen-responsive transcripts per comparison, while interconnected dots signify the transcripts shared between the two viruses. (C) Single-cell RNA-seq analysis of AR expression: (upper) UMAP visualization of the cell populations nasal HAE samples UMAP plot of the single cell RNA-seq clustering from the bronchoalveolar samples from COVID-19 and healthy control individuals. A total of 34 clusters were found in this sample of 6 severe and 3 mild COVID-19 patients as well as 3 healthy controls. Each cluster is colored differently and depicted by a number. (lower) UMAP visualization of the AR distribution in HAE. (D) Androgen response element (ARE) luciferase assay: MRC-5 cells were co-transfected with an AR expression vector and an ARE-luciferase reporter. Cells were infected with OC43 and 229E viruses, and luciferase activity was measured. The bar plot represents the luciferase activity relative to the control. Statistical significance was determined by one-way ANOVA and Tukey's post hoc tests (\* $p < 0.05$ , \*\* $p < 0.005$ , \*\*\* $p < 0.0005$ , \*\*\*\* $p < 0.0001$ ).

The AR governs the expression of target genes by binding to specific DNA elements, a process primarily facilitated by its DNA-binding domain (DBD). Upon binding with androgen, the AR translocates into the nucleus, where it forms homodimers and directly interacts with DNA, often at the consensus AR-binding motifs known as canonical androgen response element (ARE) motifs.<sup>32</sup> Our RNA-seq analyses, incorporating three well-established androgen-responsive gene signatures, revealed marked distinctions in how AR-regulated genes respond to HCoV in primary nasal epithelial cells. Notably, the enzalutamide-sensitive 229E induces alterations in a specific subset of AR-regulated transcripts, while the enzalutamide-resistant OC43 influences only a limited number, underscoring nuanced regulatory dynamics by HCoV. To dissect this complexity, we employed an ARE-luciferase construct, revealing a significant increase in luciferase activity during 229E infection in MRC-5 cells, independent of androgen stimulation, indicating a direct association between viral infection and androgen signaling. Intriguingly, OC43 infection demonstrated a contrasting effect, suppressing ARE activation with mibolerone, potentially accounting for the observed resistance in OC43-infected cells against enzalutamide.

This research contributes valuable insights into the intricate relationship between coronaviruses and androgen signaling. However, it is crucial to acknowledge certain limitations. First, the absence of clinical studies restricts the direct translation of these findings to human patients. Considering the potential application in immunocompromised individuals at early stages of infection, enzalutamide may serve as an alternative to potent antiviral drugs, acting as a preventive measure against severe outcomes or as a therapeutic option. Further investigations involving clinical data are essential to validate the relevance of these observations in real-world scenarios. Additionally, a more comprehensive examination of other androgen-regulated factors, especially across all seasonal coronaviruses, including HKU1, which is uncultivable in cell culture, would enhance our understanding of the broader impact of androgen signaling in the context of coronavirus infections. These limitations should guide future research and bridge the gap between laboratory findings and clinical applicability.

In conclusion, our study highlights the intricate relationship between viral infections and host androgen signaling. Our data suggest that viruses can manipulate androgen signaling, either by mimicking or antagonizing the AR pathway, presenting potential implications for managing viral infections and developing therapeutic interventions. Enzalutamide's inhibition of AR activity, as demonstrated in our study, may impede infection of 229E and NL63 coronaviruses through both TMPRSS2-dependent and TMPRSS2-independent pathways. Given the lack of approved antiviral drugs for seasonal coronaviruses, our research presents a potential avenue for novel therapeutic options centered around antiandrogens. Further exploration, especially through clinical trials, is essential to validate these findings and translate them into effective antiviral strategies.

## AUTHOR CONTRIBUTIONS

Oluwadamilola D. Ogunjinmi performed experiments, analysed data, and wrote the first draft of the manuscript. Tukur Abdullahi, Riaz-Ali Somji, and Efstathios S. Giotis performed experiments and analysed data. Charlotte L. Bevan, Nigel Temperton, Wendy S. Barclay, and Greg N. Brooke provided reagents and edited the manuscript; Efstathios S. Giotis conceptualised the study, supervised activities, and edited the manuscript. All authors have read and agreed to the published version of the manuscript.

## ACKNOWLEDGMENTS

We thank Aygun Azadova Adilova, Tiffany Teoh and Veronica Mavrovouna for their technical assistance. Funding was provided by the University of Essex COVID-19 Rapid and Agile and the Faculty of Science and Health Research Innovation and Support Funds. Tukur Abdullahi is supported by the Nigerian Petroleum Technology Development Fund and the University of Essex. Nigel Temperton acknowledges support from Wellcome Trust (360G-Wellcome-220981\_Z\_20\_Z).

## CONFLICT OF INTEREST STATEMENT

The authors declare no conflict of interest.

## DATA AVAILABILITY STATEMENT

The data that support the findings of this study are available from the corresponding author upon reasonable request.

## ORCID

Efstathios S. Giotis  <http://orcid.org/0000-0001-8908-7824>

## REFERENCES

1. Cui J, Li F, Shi ZL. Origin and evolution of pathogenic coronaviruses. *Nat Rev Microbiol.* 2019;17(3):181-192.
2. Ljubin-Sternak S, Meštrović T, Lukšić I, Mijač M, Vraneš J. Seasonal coronaviruses and other neglected respiratory viruses: a global perspective and a local snapshot. *Front Public Health.* 2021;9:691163.
3. Tao Y, Shi M, Chommanard C, et al. Surveillance of bat coronaviruses in Kenya identifies relatives of human coronaviruses NL63 and 229E and their recombination history. *J Virol.* 2017;91(5):e01953-16.
4. Bradburne AF, Bynoe ML, Tyrrell DA. Effects of a "new" human respiratory virus in volunteers. *BMJ.* 1967;3(5568):767-769.
5. Vassilara F, Spyridaki A, Pothitos G, Deliveliotou A, Papadopoulos A. A rare case of human coronavirus 229E associated with acute respiratory distress syndrome in a healthy adult. *Case Rep Infect Dis.* 2018;2018:1-4.
6. van der Hoek L, Sure K, Ihorst G, et al. Croup is associated with the novel coronavirus NL63. *PLoS Med.* 2005;2(8):e240.
7. Lobaina Y, Chen R, Ai P, et al. Cross-reactive profile against two conserved coronavirus antigens in sera from SARS-CoV-2 hybrid and vaccinated immune donors. *Viral Immunol.* 2023;36(3):222-228.
8. Giotis ES, Cil E, Brooke GN. Use of antiandrogens as therapeutic agents in COVID-19 patients. *Viruses.* 2022;14(12):2728.
9. Leach DA, Mohr A, Giotis ES, et al. The antiandrogen enzalutamide downregulates TMPRSS2 and reduces cellular entry of SARS-CoV-2 in human lung cells. *Nat Commun.* 2021;12(1):4068.

10. Lucas JM, Heinlein C, Kim T, et al. The androgen-regulated protease TMPRSS2 activates a proteolytic cascade involving components of the tumor microenvironment and promotes prostate cancer metastasis. *Cancer Discov.* 2014;4(11):1310-1325.
11. Cadegiani FA, Goren A, Wambier CG. Spironolactone may provide protection from SARS-CoV-2: targeting androgens, angiotensin converting enzyme 2 (ACE2), and renin-angiotensin-aldosterone system (RAAS). *Med Hypotheses.* 2020;143:110112.
12. Baratchian M, McManus JM, Berk MP, et al. Androgen regulation of pulmonary AR, TMPRSS2 and ACE2 with implications for sex-discordant COVID-19 outcomes. *Sci Rep.* 2021;11(1):11130.
13. Yeager CL, Ashmun RA, Williams RK, et al. Human aminopeptidase N is a receptor for human coronavirus 229E. *Nature.* 1992;357(6377):420-422.
14. Hofmann H, Pirc K, van der Hoek L, Geier M, Berkhout B, Pöhlmann S. Human coronavirus NL63 employs the severe acute respiratory syndrome coronavirus receptor for cellular entry. *Proc Natl Acad Sci.* 2005;102(22):7988-7993.
15. Huang X, Dong W, Milewska A, et al. Human coronavirus HKU1 spike protein uses O-acetylated sialic acid as an attachment receptor determinant and employs hemagglutinin-esterase protein as a receptor-destroying enzyme. *J Virol.* 2015;89(14):7202-7213.
16. Saunders N, Fernandez I, Planchais C, et al. TMPRSS2 is a functional receptor for human coronavirus HKU1. *Nature.* 2023;624(7990):207-214.
17. Belouzard S, Millet JK, Licitra BN, Whittaker GR. Mechanisms of coronavirus cell entry mediated by the viral spike protein. *Viruses.* 2012;4(6):1011-1033.
18. Shirato K, Kanou K, Kawase M, Matsuyama S. Clinical isolates of human coronavirus 229E bypass the endosome for cell entry. *J Virol.* 2017;91(1):e01387-16.
19. Bertram S, Dijkman R, Habjan M, et al. TMPRSS2 activates the human coronavirus 229E for cathepsin-independent host cell entry and is expressed in viral target cells in the respiratory epithelium. *J Virol.* 2013;87(11):6150-6160.
20. Matoba Y, Aoki Y, Tanaka S, et al. HeLa-ACE2-TMPRSS2 cells are useful for the isolation of human coronavirus 229E. *Jpn J Infect Dis.* 2016;69(5):452-454.
21. Milewska A, Nowak P, Owczarek K, et al. Entry of human coronavirus NL63 into the cell. *J Virol.* 2018;92(3):e01933-17.
22. Giotis ES, Carnell G, Young EF, et al. Entry of the bat influenza H17N10 virus into mammalian cells is enabled by the MHC class II HLA-DR receptor. *Nat Microbiol.* 2019;4(12):2035-2038.
23. Rihn SJ, Merits A, Bakshi S, et al. A plasmid DNA-launched SARS-CoV-2 reverse genetics system and coronavirus toolkit for COVID-19 research. *PLoS Biol.* 2021;19(2):e3001091.
24. Sampson AT, Heeney J, Cantoni D, et al. Coronavirus pseudotypes for all circulating human coronaviruses for quantification of cross-neutralizing antibody responses. *Viruses.* 2021;13(8):1579.
25. Hu Y, Ma C, Wang J. Cytopathic effect assay and plaque assay to evaluate in vitro activity of antiviral compounds against human coronaviruses 229E, OC43, and NL63. *Bio-Protocol.* 2022;12(3):e4314.
26. Loo SL, Wark PAB, Esneau C, Nichol KS, Hsu ACY, Bartlett NW. Human coronaviruses 229E and OC43 replicate and induce distinct antiviral responses in differentiated primary human bronchial epithelial cells. *Am J Physiol Lung Cell Mol Physiol.* 2020;319(6):L926-L931.
27. Giotis ES, Ross CS, Robey RC, Nohturfft A, Goodbourn S, Skinner MA. Constitutively elevated levels of SOCS1 suppress innate responses in DF-1 immortalised chicken fibroblast cells. *Sci Rep.* 2017;7(1):17485.
28. Giotis ES, Laidlaw SM, Bidgood SR, et al. Modulation of early host innate immune response by an Avipox vaccine virus' lateral body protein. *Biomedicines.* 2020;8(12):634.
29. Zhang Z, Penn R, Barclay WS, Giotis ES. Naïve human macrophages are refractory to SARS-CoV-2 infection and exhibit a modest inflammatory response early in infection. *Viruses.* 2022;14(2):441.
30. Giotis ES, Montillet G, Pain B, Skinner MA. Chicken embryonic-stem cells are permissive to poxvirus recombinant vaccine vectors. *Genes.* 2019;10(3):237.
31. Brooke GN, Powell SM, Lavery DN, et al. Engineered repressors are potent inhibitors of androgen receptor activity. *Oncotarget.* 2014;5(4):959-969.
32. Mikkonen L, Pihlajamaa P, Sahu B, Zhang FP, Jänne OA. Androgen receptor and androgen-dependent gene expression in lung. *Mol Cell Endocrinol.* 2010;317(1-2):14-24.
33. Moreira ÉA, Locher S, Kolesnikova L, et al. Synthetically derived bat influenza A-like viruses reveal a cell type- but not species-specific tropism. *Proc Natl Acad Sci.* 2016;113(45):12797-12802.
34. Jiang D, Schaefer N, Chu HW. Air-liquid interface culture of human and mouse airway epithelial cells. *Methods Mol Biol.* 2018;1809:91-109.
35. Tse BWC, Volpert M, Rattner E, et al. Neuropilin-1 is upregulated in the adaptive response of prostate tumors to androgen-targeted therapies and is prognostic of metastatic progression and patient mortality. *Oncogene.* 2017;36(24):3417-3427.
36. Samuel RM, Majd H, Richter MN, et al. Androgen signaling regulates SARS-CoV-2 receptor levels and is associated with severe COVID-19 symptoms in men. *Cell Stem Cell.* 2020;27(6):876-889.
37. Xie Y, Wang L, Khan MA, et al. Metformin and androgen receptor-axis-targeted (ARAT) agents induce two PARP-1-dependent cell death pathways in androgen-sensitive human prostate cancer cells. *Cancers.* 2021;13(4):633.
38. Nelson PS, Clegg N, Arnold H, et al. The program of androgen-responsive genes in neoplastic prostate epithelium. *Proc Natl Acad Sci.* 2002;99(18):11890-11895.
39. Doane AS, Danso M, Lal P, et al. An estrogen receptor-negative breast cancer subset characterized by a hormonally regulated transcriptional program and response to androgen. *Oncogene.* 2006;25(28):3994-4008.
40. Liberzon A, Birger C, Thorvaldsdóttir H, Ghandi M, Mesirov JP, Tamayo P. The molecular signatures database hallmark gene set collection. *Cell Systems.* 2015;1(6):417-425.
41. Townsend JP, Hassler HB, Lamb AD, et al. Seasonality of endemic COVID-19. *mBio.* 2023;14(6):e0142623.
42. Alchikh M, Conrad T, Hoppe C, et al. Are we missing respiratory viral infections in infants and children? Comparison of a hospital-based quality management system with standard of care. *Clin Microbiol Infect.* 2019;25(3):380.e9-380.e16.
43. Yousefi B, Valizadeh S, Ghaffari H, Vahedi A, Karbalaeei M, Eslami M. A global treatments for coronaviruses including COVID-19. *J Cell Physiol.* 2020;235(12):9133-9142.
44. Brooke GN, Gamble SC, Hough MA, et al. Antiandrogens act as selective androgen receptor modulators at the proteome level in prostate cancer cells. *Mol Cell Proteomics.* 2015;14(5):1201-1216.
45. Koch J, Uckelely ZM, Doldan P, Stanifer M, Boulant S, Lozach PY. TMPRSS2 expression dictates the entry route used by SARS-CoV-2 to infect host cells. *EMBO J.* 2021;40(16):e107821.
46. Chiu CM, Yeh SH, Chen PJ, et al. Hepatitis B virus X protein enhances androgen receptor-responsive gene expression depending on androgen level. *Proc Natl Acad Sci.* 2007;104(8):2571-2578.

47. Sawant L, Thunuguntla P, Jones C. Cooperative activation of bovine herpesvirus 1 productive infection and viral regulatory promoters by androgen receptor and Krüppel-like transcription factors 4 and 15. *Virology*. 2021;552:63-72.

#### SUPPORTING INFORMATION

Additional supporting information can be found online in the Supporting Information section at the end of this article.

**How to cite this article:** Ogunjinmi OD, Abdullahi T, Somji R-A, et al. The antiviral potential of the antiandrogen enzalutamide and the viral-androgen signalling interplay in seasonal coronaviruses. *J Med Virol*. 2024;96:e29540. doi:10.1002/jmv.29540